




MODELLING AND SIMULATION STUDY OF CONVENTIONAL FACTS-CONTROLLERS



 Crescent
Onyebuchi Omeje

Department of Electrical/Electronic Engineering, University of Port
Harcourt, Rivers State Nigeria.
Email: crescent.omeje@uniport.edu.ng Tel: +2348032645484



ABSTRACT

Article History

Received: 19 September 2019

Revised: 25 October 2019

Accepted: 2 December 2019

Published: 7 January 2020

Keywords

Thyristor controlled reactor
Static Var compensator
Unified power flow controller
Closed loop control system
Pulse width modulator
Reactive power losses
MATLAB simulation.

This paper presents a comparative analysis of basic forms of Flexible Alternating Current Transmission Systems (FACTS) Devices. The effect of thyristor firing angle on the transmitted voltage and current by the Thyristor Controlled Reactor (TCR) is presented. The real and the reactive power produced by the Thyristor Controlled Reactor at $L = 100\text{mH}$ is also presented. The rate of reactive power absorption and injection on the transmission line by two selected FACTS-Devices such as the Static Var Compensator (SVC) and the Unified Power Flow Controller (UPFC) is mathematically modeled and evaluated with respect to a regulated voltage and current magnitude. Simulation results carried out on the circuit models indicate that Thyristor Controlled Reactor absorbed more reactive power of 1.875KVAR with a reduced overload. The Static Var Compensator injected more reactive power of 28.75KVAR to the transmission line while the Unified Power Flow Controller reduced excess overload through phase angle adjustment with the injection of less reactive power of 675VAR to the transmission line grid. All simulations were actualized in MATLAB 7.14 version.

Contribution/ Originality: This study applied a new methodology in evaluating the rate of reactive power injection and absorption into the transmission line grid network using three conventional FACTS-Controllers. Power equations were formulated and simulated. The simulation results indicated that TCR absorbed more reactive power while SVC injected more reactive power to the transmission line with a reduced overload.

1. INTRODUCTION

A flexible alternating current transmission systems (FACTS) device is a recent technological development in electrical power systems. Its operation is based on high-power semi-conductor device technology. The early development of the FACTS technology is observed in power electronic version of the phase-shifting and tap-changing transformers [1]. These controllers together with the electronic series compensator can be considered to belong to the first generation of FACTS equipment [1]. The unified power flow controller (UPFC), the static var compensator (SVC) and some inter-phased power controllers are the most recent developments. Their control capabilities and intended functions are more sophisticated than those of the first wave of FACTS controllers [2]. The recent emerging power electronics applications in power systems as referenced in Hingorani and Gyugyi [3] are classified as: (i) Bulk active and reactive power control (ii) Voltage quality improvement. The first application is a FACTS based application where the latest power electronic devices and methods are used to control the high

voltage transmission electronically [3]. The second application focuses on the low voltage distribution and is created in response to the poor power quality and reliability of supply affecting most industries and homes [3].

2. THYRISTOR CONTROLLED REACTOR (TCR)

Power electronic circuits using conventional thyristors have been widely applied in power transmission application in the early 1970 [4]. The first application was on the high voltage direct current (HVDC) transmission network [4]. More recently, fast acting series compensator using thyristors have been applied to vary the electrical length of key transmission lines with a negligible delay angle [5]. In distribution system applications, solid state transfer switching using thyristors are being utilized to enhance the reliability of supply to critical customer load [6]. The main component of the basic thyristor controlled reactor (TCR) is shown in Figure 1. The controllable element is the anti-parallel thyristor pair Th1 and Th2 which conducts on alternate half cycle of the supply frequency. The thyristor conduction is dependent on the firing angle as represented in Equation 1.

$$\sigma = 2(\pi - \alpha) \tag{1}$$

Where: σ = conduction angle and α = thyristor firing angle.

Partial conduction of the thyristor is achieved when the firing angle fall in the range of $\frac{\pi}{2} < \alpha < \pi$. This implies that increasing the value of the firing angle above $\frac{\pi}{2}$ causes the TCR current waveform to become non-sinusoidal with the fundamental frequency component reduced in magnitude.

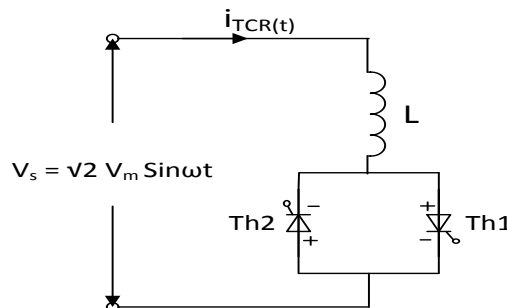


Figure-1. Basic thyristor controlled reactor [2].
Source: Fuerte-Esquivel, et al. [2].

The instantaneous thyristor current $i_{TCR}(t)$ is given by Equation 2.

$$i_{TCR}(t) = \frac{1}{L} \int_{\alpha}^{\omega t} \sqrt{2} V_m \sin \omega t \, dt = \frac{\sqrt{2}}{\omega L} (\cos \alpha - \cos \omega t) \tag{2}$$

An expression for the fundamental frequency current I_{TCRF1} is given by Equation 3.

$$I_{TCRF1} = \frac{V_m}{j\omega L \pi} [2(\pi - \alpha) + \sin 2\alpha] = \frac{V_m}{j\omega L \pi} (\sigma + \sin 2\alpha) \tag{3}$$

Where : σ = conduction angle, α = firing angle and V_m = peak voltage.

The overall action of the thyristor controller on the linear reactor is to act as a controllable susceptance in the inductive sense as presented in Equation 4.

$$i_{TCR} = -jB_{TCR}V \tag{4}$$

$$B_{TCR} = \frac{2(\pi - \alpha) + \sin 2\alpha}{\omega L\pi} \tag{5}$$

In power system, TCR installations are usually three-phase based. Filters and other harmonic cancellation arrangements are used to prevent the harmonic currents from reaching the high-voltage terminal of the network. Figure 2 shows a three-phase, delta connected TCR. This topology uses six groups of thyristor and is commonly known as a six-pulse thyristor controlled reactor (TCR).

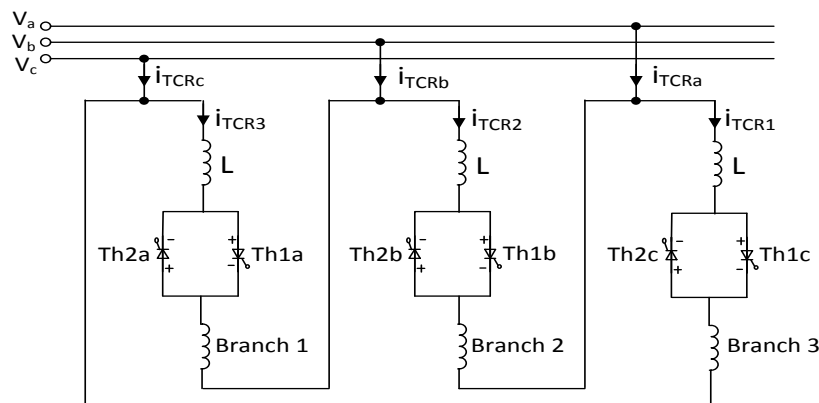


Figure-2. Three-phase thyristor controlled reactor (TCR) [2].
Source: Fuerte-Esquivel, et al. [2].

The three phase thyristor current in terms of the nodal admittance is represented in Equation 6

$$\begin{bmatrix} i_{TCR1} \\ i_{TCR2} \\ i_{TCR3} \end{bmatrix} = \begin{bmatrix} -jB_{TCR1} & 0 & 0 \\ 0 & -jB_{TCR2} & 0 \\ 0 & 0 & -jB_{TCR3} \end{bmatrix} \times \begin{bmatrix} V_1 \\ V_2 \\ V_3 \end{bmatrix} \tag{6}$$

Where:

$$\begin{bmatrix} V_1 \\ V_2 \\ V_3 \end{bmatrix} = \frac{(-\pi)}{\sqrt{3}} \times \begin{bmatrix} 1 & 0 & -1 \\ -1 & 1 & 0 \\ 0 & -1 & 1 \end{bmatrix} \times \begin{bmatrix} V_a \\ V_b \\ V_c \end{bmatrix} \tag{7}$$

$$V_a = V_m \sin \omega t \tag{8}$$

$$V_b = V_m \sin \left(\omega t - \frac{2\pi}{3} \right) \tag{9}$$

$$V_c = V_m \sin \left(\omega t - \frac{4\pi}{3} \right) \tag{10}$$

$$\begin{bmatrix} i_{TCRa} \\ i_{TCRb} \\ i_{TCRc} \end{bmatrix} = \frac{(-\pi)}{\sqrt{3}} \begin{bmatrix} 1 & 0 & -1 \\ -1 & 1 & 0 \\ 0 & -1 & 1 \end{bmatrix} \times \begin{bmatrix} i_{TCR1} \\ i_{TCR2} \\ i_{TCR3} \end{bmatrix} \tag{11}$$

Substituting (7) into (6) and also the resultant intermediate equation into (11) gives rise to (12).

$$\begin{bmatrix} i_{TCRa} \\ i_{TCRb} \\ i_{TCRc} \end{bmatrix} = \frac{1}{3} \begin{bmatrix} -j(B_{TCR1} + B_{TCR2}) & jB_{TCR1} & jB_{TCR3} \\ jB_{TCR1} & -j(B_{TCR1} + B_{TCR2}) & jB_{TCR2} \\ jB_{TCR3} & jB_{TCR2} & -j(B_{TCR2} + B_{TCR3}) \end{bmatrix} \times \begin{bmatrix} V_a \\ V_b \\ V_c \end{bmatrix} \quad (12)$$

If all the three branches in the TCR have equal equivalent susceptances ($B_{TCR1} = B_{TCR2} = B_{TCR3} = B_{TCR}$) under this condition, (12) transforms into (13).

$$\begin{bmatrix} i_{TCRa} \\ i_{TCRb} \\ i_{TCRc} \end{bmatrix} = \frac{1}{3} \begin{bmatrix} -j2B_{TCR} & jB_{TCR} & jB_{TCR} \\ jB_{TCR} & -j2B_{TCR} & jB_{TCR} \\ jB_{TCR} & jB_{TCR} & -j2B_{TCR} \end{bmatrix} \times \begin{bmatrix} V_a \\ V_b \\ V_c \end{bmatrix} \quad (13)$$

The apparent power for the thyristor controlled reactor is presented in (14).

$$S_{Ga} = i_{TCRa} \times V_a = P + jQ \quad (14)$$

Where: P = Real or useful power (VA) and Q = Reactive power (VAR).

3. STATIC VAR COMPENSATOR (SVC)

The static var compensator is a power electronics based power factor, voltage and current regulating device [7, 8]. The SVC is usually connected in shunt or in series to the a.c transmission or distribution grid network [9-11]. In its simplest form and from operational view point, the SVC acts like a shunt-connected variable reactance which can either generate or absorb reactive power so as to regulate the voltage magnitude at the point of common coupling (PCC) [12-14]. It is extensively used to provide fast reactive power and voltage regulation support [15, 16]. The one-line diagram of the grid connected static VAR compensator is represented in two forms as shown in Figures 3 and 4.

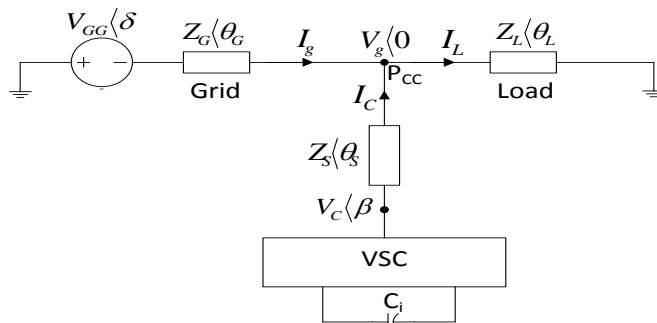


Figure-3. One line diagram of grid connected static VAR compensator with a capacitor source [16].

Source: Agu [16].

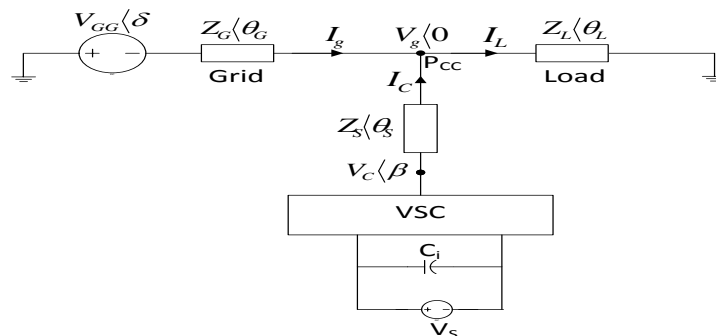


Figure-4. One Line diagram of Grid connected Static VAR Compensator with a Capacitor and active voltage Source [16].

Source: Agu [16].

When a dc voltage source is connected across the input capacitor, the static var compensator in addition to being able to exchange reactive power with the a.c grid can also supply some active power to the grid. The apparent power injected to the grid by the static var compensator and the apparent power supplied to the grid can be determined from Equation 15-20.

$$I_c = \frac{V_c(\beta - V_g \angle 0)}{Z_s \angle \theta_s} \quad (14)$$

Apparent power delivered by the static var compensator to the grid is given by Equation 15:

$$S_{c\bar{g}} = V_{\bar{g}} \times I_c^* = P_{c\bar{g}} + jQ_{c\bar{g}} \quad (15)$$

$$P_{c\bar{g}} = \frac{V_{\bar{g}}}{Z_s} (V_c \cos(\theta_s - \beta) - V_{\bar{g}} \cos \theta_s) \quad (16)$$

$$Q_{c\bar{g}} = \frac{V_{\bar{g}}}{Z_s} (V_c \sin(\theta_s - \beta) - V_{\bar{g}} \sin \theta_s) \quad (17)$$

Where: $P_{c\bar{g}}$ and $Q_{c\bar{g}}$ represent the active power and reactive power delivered by the static var compensator to the a.c grid. The apparent power $S_{\bar{g}}$ from the grid to the point of common coupling (PCC) is given by Equation 18.

$$S_{\bar{g}} = V_{\bar{g}} I_{\bar{g}}^* = V_{\bar{g}} (I_L - I_c)^* = V_{\bar{g}} \left(\frac{V_g}{Z_s \angle \theta_s} - \frac{V_c(\beta - V_g \angle 0)}{Z_s \angle \theta_s} \right)^* \quad (18)$$

Further simplification of Equation 18 gives rise to Equation 19.

$$S_{\bar{g}} = P_{\bar{g}} + jQ_{\bar{g}} \quad (19)$$

Where:

$$P_{\bar{g}} = V_{\bar{g}} \left(\frac{V_g \cos \theta_L}{Z_L} - \frac{1}{Z_s} (V_c \cos(\theta_s - \beta) - V_{\bar{g}} \cos \theta_s) \right) \quad (20)$$

$$Q_{\bar{g}} = V_{\bar{g}} \left(\frac{V_g \sin \theta_L}{Z_L} - \frac{1}{Z_s} (V_c \sin(\theta_s - \beta) - V_{\bar{g}} \sin \theta_s) \right) \quad (21)$$

$P_{\bar{g}}$ and $Q_{\bar{g}}$ are the respective active and reactive powers delivered to the static var compensator and load by the grid. The static var compensator (SVC) can only exchange reactive power with the grid. It is usually operated in such a way that the grid supplies the real power component needed by the load while itself (SVC) injects or absorbs the load reactive power. This implies that $Q_{\bar{g}}$ is maintained at zero by varying phase angle β under varying load conditions. If the series link inductor L_s of quality factor $\frac{\omega_g L_s}{R_s}$ is sufficiently high, the phase angle β will be small

such that it can be assumed to be $\theta_s = \frac{\pi}{2}$, $\cos \beta = 1$ and $\sin \beta = \beta$ radians under this condition, the active power

P_{cg} in Equation 16 becomes negligible while the reactive power Q_{cg} delivered by the compensator to the grid is approximated to Equation 22.

$$Q_{cg} = \frac{V_g}{Z_s} (V_c - V_g) \tag{22}$$

It can be deduced from Equation 22 that when the compensator voltage $V_c > V_g$, Q_{cg} will always be positive indicating that the compensator delivers reactive power to the grid. Conversely, when the compensator voltage $V_c < V_g$, Q_{cg} will always be negative indicating that the compensator absorbs reactive power from the grid. Reactive power flows from the compensator to the grid if the load is inductive ($R_L + jQ_L$) while reactive power flows from the grid to the compensator if the load is capacitive ($R_L - jQ_L$). The complete circuit diagram of a three phase three-level voltage source converter based static var compensator for three phase grid system is presented in Figure 5.

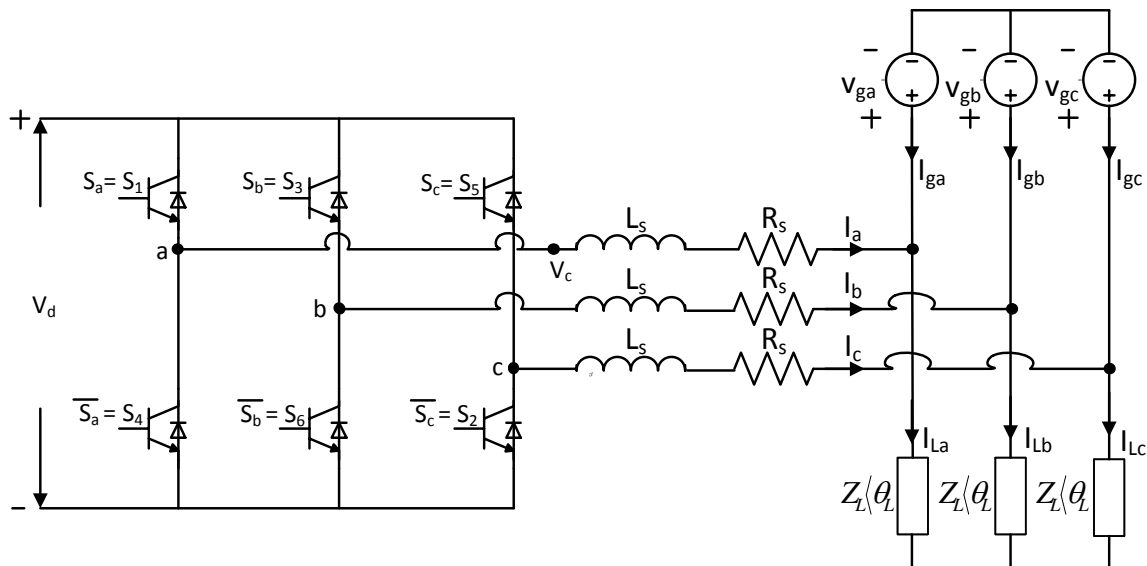


Figure-5. Three level voltage source converter based SVC for three phase grid system [16].
Source: Agu [16].

3.1. Unity Power Factor Control Scheme of the Static VAR Compensator (SVC)

A closed loop control arrangement that maintains the grid power factor at unity value ($Q_g = 0$) under a load varying condition is presented in Figure 6. The grid reference or default reactive power ($Q_{ref} = 0$) is summed with the grid feedback reactive power Q_{gF} to produce a grid reactive power error ($Q_{gref} - Q_{gF}$). The error generated is adjusted with the proportional integral controller to produce the phase angle difference β of the compensator output voltage V_c relative to the grid voltage V_g . The phase angle difference β is added to the time varying phase $\omega_g t$ of the instantaneous grid voltage resulting to a new phasor ($\beta + \omega_g t$) which is applied in the modulating signal of the

SVC pulse-width modulator to generate the SVC switching signals for Figure 5. The feedback grid reactive power Q_{gF} is obtained by low pass filtering of the product of the grid current and voltage as shown in Figure 6. Q_{gF} is represented by Equation 23.

$$Q_{gF} = I_g \times V_g = -[V_g I_g \sin \theta_g + V_g I_g \sin(2\omega_g t + \theta_g)] \quad (23)$$

The low pass filter suppresses the high frequency component of Equation 23 to form Equation 24.

$$Q_{gF} = -V_g I_g \sin \theta_g \quad (24)$$

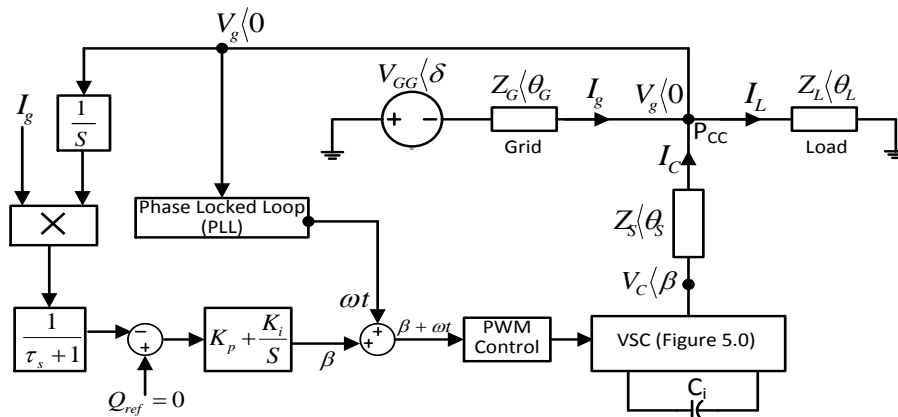


Figure-6. Closed loop control block diagram of three-level voltage source converter based SVC [15, 16]. Source: Agu [16].

4. UNIFIED POWER FLOW CONTROLLER (UPFC)

The unified power flow controller (UPFC) also termed as the unified power quality conditioner (UPQC) amongst other FACTS devices is the most widely applied device in power factor correction [17-22]. The UPFC is capable of selectively controlling all the transmission line parameters which include voltage magnitude, line impedance and voltage/current phase angle [23, 24]. The conventional UPFC consists of two back to back voltage source converters (Rectifier and Inverter). They share a common dc link (V_{dc}) as shown in Figure 7. The transmission line shunt and series connected transformers (TR_{shunt} and TR_{series}) provide galvanic isolation to the respective input/output of the back to back converter. The voltage V_{so} is the transmission line sending end voltage while V_R is the receiving end voltage. The current I_{shunt} drawn from the transmission line by the shunt transformer is a controllable current source while the voltage V_c induced in the transmission line by the series transformer is a controllable voltage source. Both I_{sh} and V_c are controlled by the modulated back to back connected voltage source inverter.

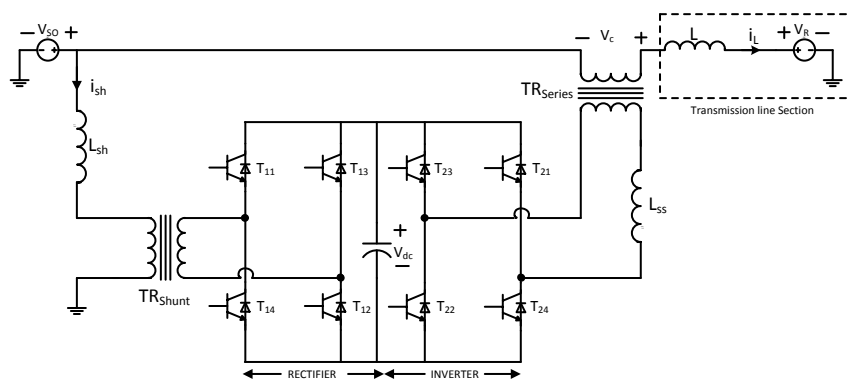


Figure-7. Conventional single phase unified power flow controller [24]. Source: Khadikar and Chandra [24].

The controllable input current i_{shunt} into the back to back connected converters is usually much smaller than the relatively large transmission line current i_L . The transmission line current with the input shunt current neglected is given by Equation 25.

$$i_L(\delta_L) = \frac{V_{s0}(\delta_{s0}) + V_c(\delta_c) - V_R(\delta_R)}{jX_L} \quad (25)$$

The real and reactive power $P + jQ$ delivered to the receiving end voltage is the product of V_R and the transmission line current conjugate.

$$P + jQ = V_R(\delta_R) \times (i_L(\delta_L))^* = V_R(\delta_R) \left(\frac{V_{s0}(\delta_{s0}) + V_c(\delta_c) - V_R(\delta_R)}{jX_L} \right)^* \quad (26)$$

Simplifying Equation 26 in Cartesian form gives rise to Equation 27.

$$P + jQ = \frac{-V_{s0}V_R \sin \delta_R}{X_L} - \frac{V_cV_R \sin(\delta_R - \delta_c)}{X_L} + j \left(\frac{V_{s0}V_R \cos \delta_R - V_R^2}{X_L} + \frac{V_cV_R \cos(\delta_R - \delta_c)}{X_L} \right) \quad (27)$$

When the compensator is not incorporated on the transmission line system (uncompensated condition), $V_c = 0$ and $\delta_c = 0$. The uncompensated transmission line system power delivered to the receiving end voltage is then represented by Equation 28.

$$P_0 + jQ_0 = \frac{-V_{s0}V_R \sin \delta_R}{X_L} + j \left(\frac{V_{s0}V_R \cos \delta_R - V_R^2}{X_L} \right) \quad (28)$$

The expression in Equation 27 is represented in a more compact form as shown in Equation 29.

$$P + jQ = P_0 + P_c + j(Q_0 + Q_c) \quad (29)$$

Where P_c and Q_c are the compensating power delivered to the receiving end voltage.

$$P_c = - \frac{V_cV_R \sin(\delta_R - \delta_c)}{X_L} \quad (30)$$

$$Q_c = \frac{V_cV_R \cos(\delta_R - \delta_c)}{X_L} \quad (31)$$

It is obvious that by selectively varying V_c and δ_c for a specified value of V_R and δ_R , the compensating power delivered to the receiving end voltage can readily be varied.

For a UPFC based electric power transmission line system where $V_{s0} = V_R$ and $\delta_R = 0$, the power delivered to the receiving end voltage can be varied if δ_c varies from 0 to $\frac{\pi}{2}$.

If $\delta_c = 0$ and $\delta_R = 0$, only reactive power is obtained from Equation 27. Similarly, if $\delta_R = \delta_c = 0$, real and reactive power are obtained but when $\delta_R = \delta_c = \frac{\pi}{2}$ only a real power is obtained.

5. SIMULATION RESULTS AND DISCUSSION

The simulation results of a single phase thyristor controlled reactor (TCR) presented in Figures 8-13 depict the characteristics waveforms of voltage and current at a varied firing angle (α) and linear reactor (L). Figure 8 showed that the current conduction span is achievable when the controlled firing angle is exceeded. At this condition, the average output voltage takes the form of the supply voltage within the span of thyristor conduction. The average output voltage drop below the negative half cycle is a consequence of the residual energy stored in the linear reactor as the thyristor is set into conduction. During conduction, the thyristor voltage V_{AK} is usually set to a zero value as a result of internal short circuit. This phenomenon is represented in Figure 9. The average output current and voltage increases in magnitude and in electrical span length at a reduced value of the thyristor firing angle ($\alpha = 30^\circ$) and reduced linear reactor ($L = 10mH$). This is shown in Figure 10 as opposed to Figure 8. The complementary switching signals are shown in Figure 11 while the inverse function relationship between the conduction angle σ and firing angle α is shown in Figure 12. The real and reactive power obtained for the thyristor controlled reactor (TCR) is presented in Figure 13. It is evidently shown that the TCR absorbs a reactive power of 1.875KVAR at steady state and injects a real power of 2.575KW on the transmission line network. The three phase voltage and current characteristics of the static var compensator are shown in Figures 14-16. These waveforms showed that the grid voltage and current tends to be in phase when compensated. Similarly, a pulsating reactive power of 28.75KVAR is injected into the transmission line grid whereas a real power of 26.12KW is absorbed from the grid to reduce overload as shown in Figures 17-18. The plots for the unified power flow controller (UPFC) are presented in Figures 19-22. A close observation of Figure 19 which represents the sending end section shows that the shunt current is very negligible and has no significant effect on the entire network. The series current and compensator voltage at the point of common coupling indicates a better current and voltage regulation as presented in Figure 20. The receiving end section shown in Figure 21 indicates that the voltage and current are almost in phase. The receiving end voltage $V_{receive}$ has the same value with the sending voltage V_{send} which indicates a maximum voltage transmission along the grid. The real and reactive power plot in Figure 22 shows that a real power of 425Watts is absorbed by the UPFC while a reactive power of 675VAR is injected into the grid to compensate for the voltage drop in $V_c = 185.5V$. The basic functions of the selected FACTS controllers are encapsulated in Table 1.

Table-1. Basic FACTS controllers and function [24].

Facts Controllers	Functions
Thyristor Controlled Reactor (TCR)	Absorbs reactive power and reduces overload
Static Var Compensator (SVC)	Injects reactive power
Unified Power Flow Controller (UPFC)	Reduces overload through phase angle adjustment

Source: Khadikar and Chandra [24].

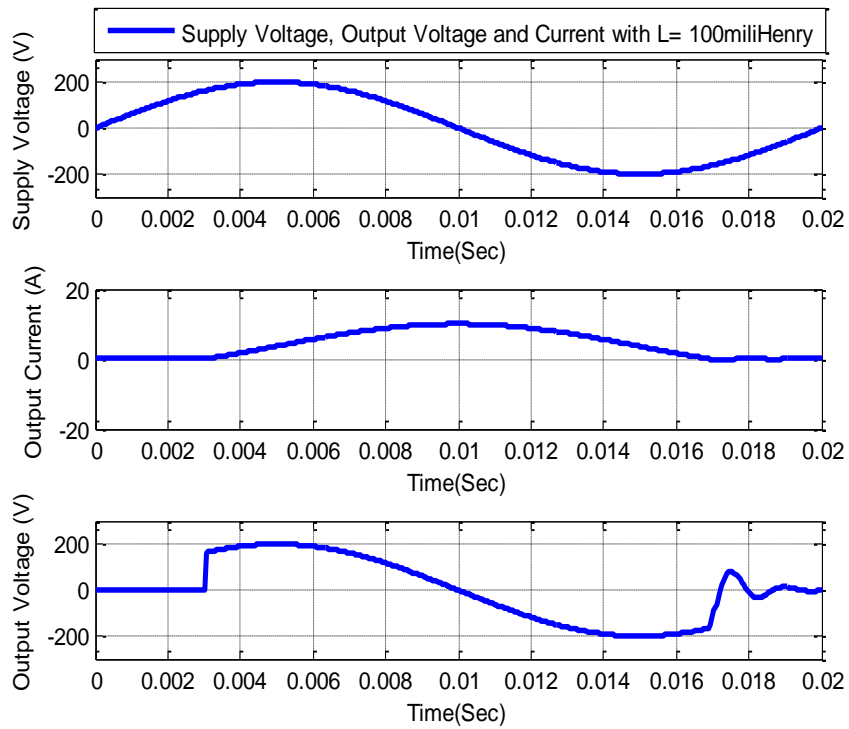


Figure-8. Plot of supply voltage, output voltage and current with $L = 100\text{mH}$ and $\alpha = 60^\circ$.
Source: Simulation result.

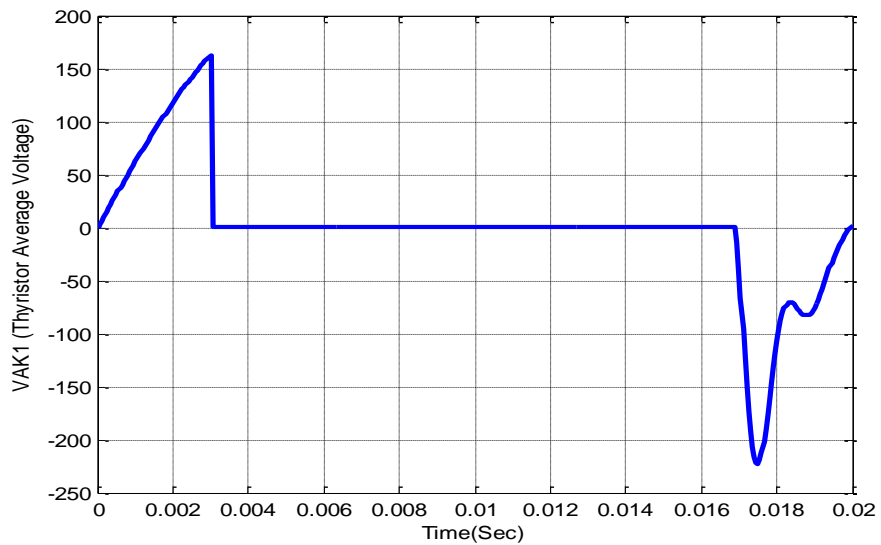


Figure-9. Plot of thyristor average voltage against time with $L = 100\text{mH}$ and $\alpha = 60^\circ$.
Source: Simulation result.

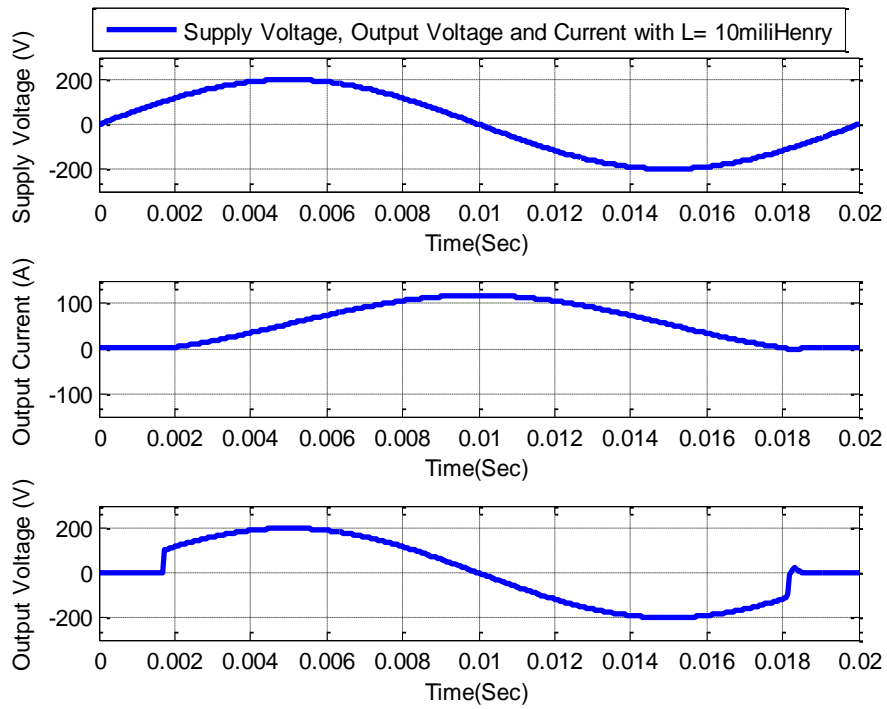


Figure-10. Plot of supply voltage, output voltage and current with $L = 10\text{mH}$ and $\alpha = 30^\circ$.
Source: Simulation result.

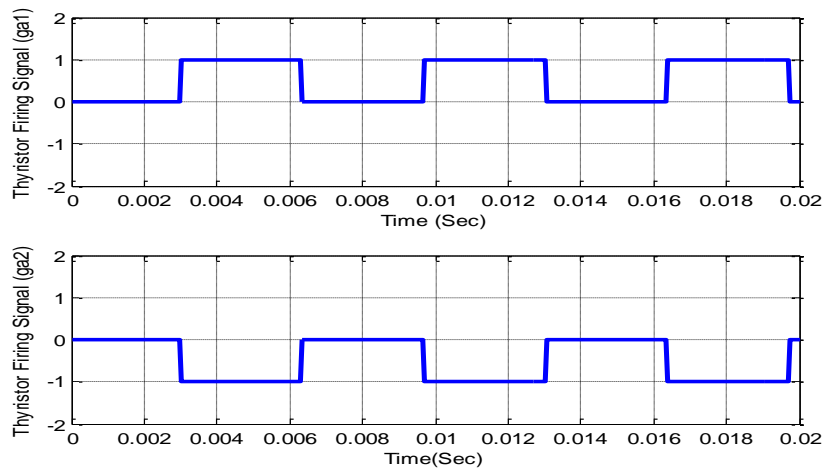


Figure-11. Plot of firing signals (IG1 and IG2) against time with 60° delay angle.
Source: Simulation result.

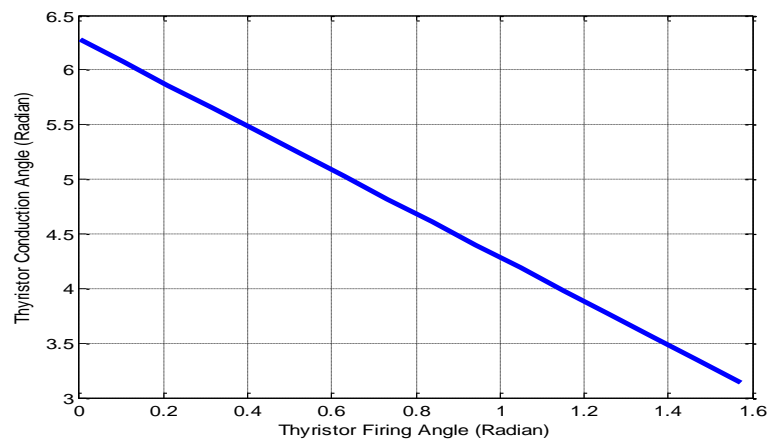


Figure-12. Plot of Thyristor Conduction Angle against the Firing angle.
Source: Simulation result.

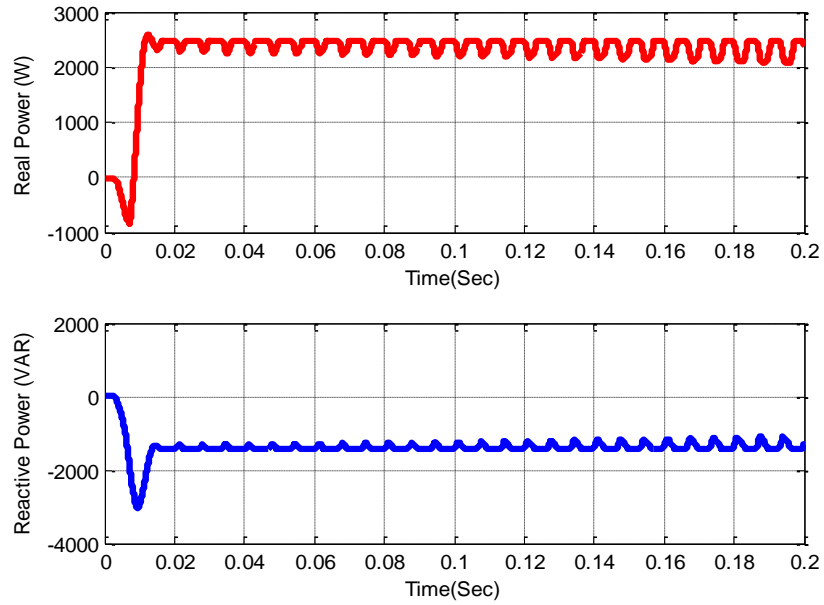


Figure-13. Plot of real and reactive power of thyristor controlled Reactor with $L = 100\text{mH}$.
Source: Simulation result.

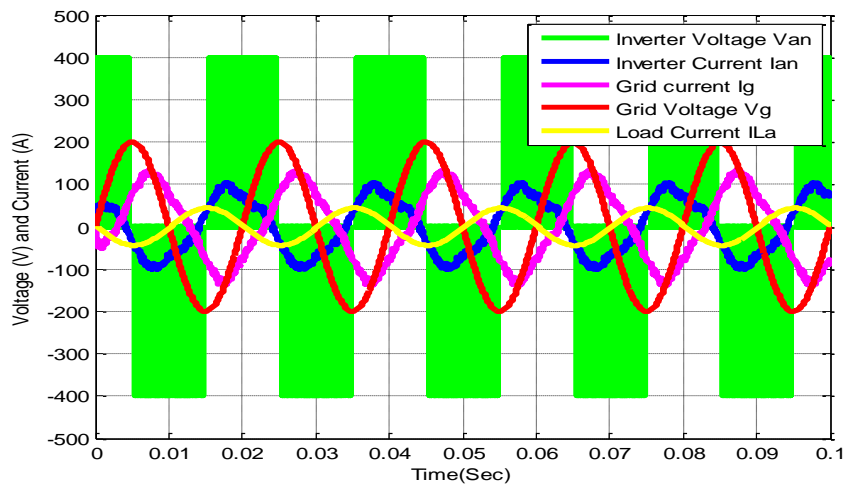


Figure-14. Plot of SVC phase (A) voltages and currents against time.
Source: Simulation result.

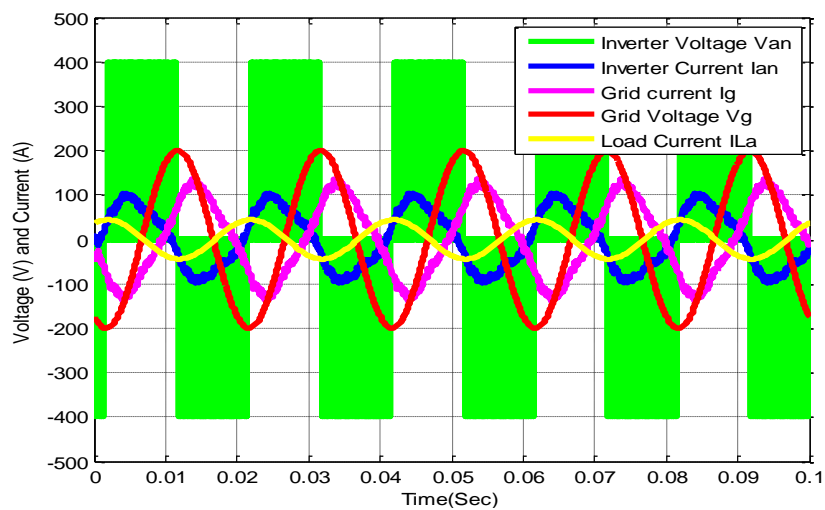


Figure-15. Plot of SVC phase (B) voltages and currents against time.
Source: Simulation result.

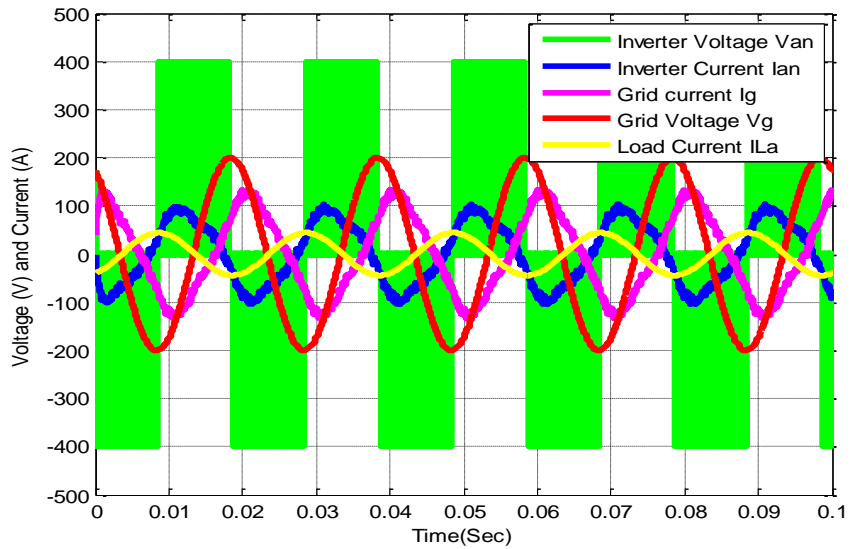


Figure-16. Plot of SVC phase (C) voltages and currents against time.

Source: Simulation result.

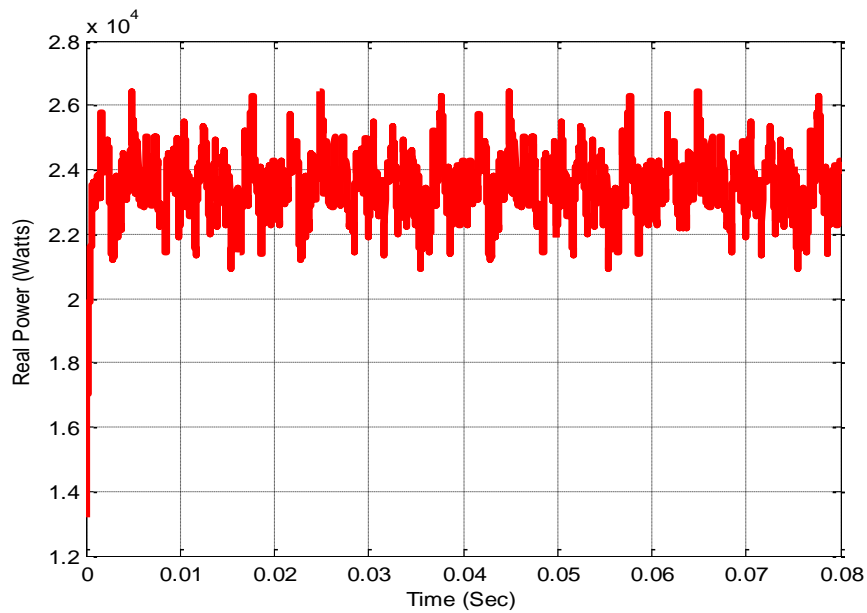


Figure-17. Plot of SVC real power with an RL load of 30Ω and 45mH.

Source: Simulation result.

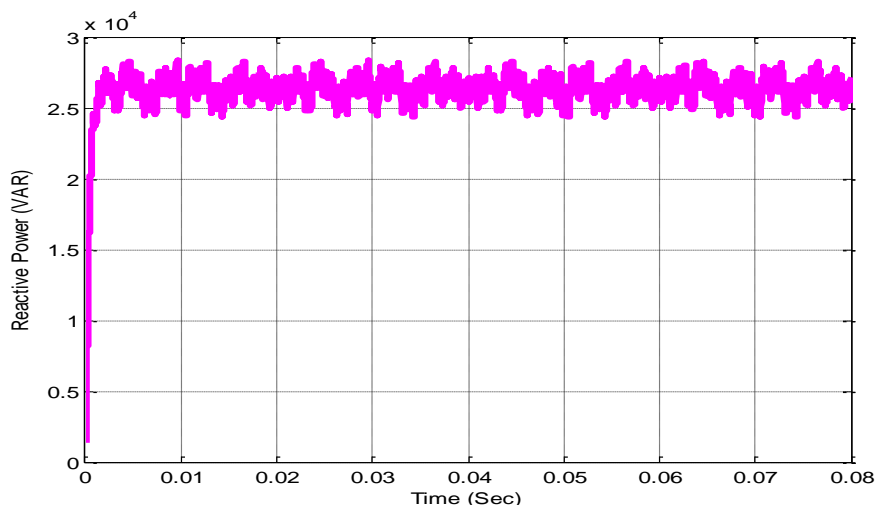


Figure-18. Plot of SVC reactive power with an RL load of 30Ω and 45mH.

Source: Simulation result.

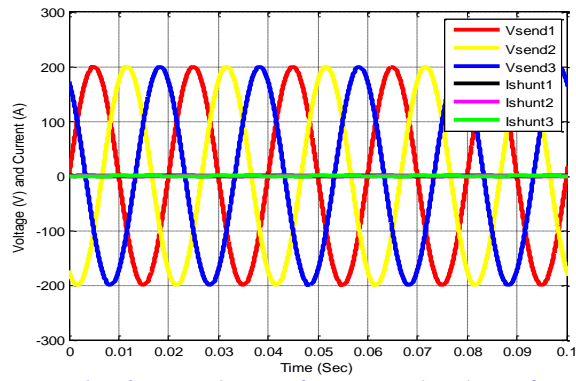


Figure-19. Plot of UPFC voltages and currents against time at the sending end.
Source: Simulation result.

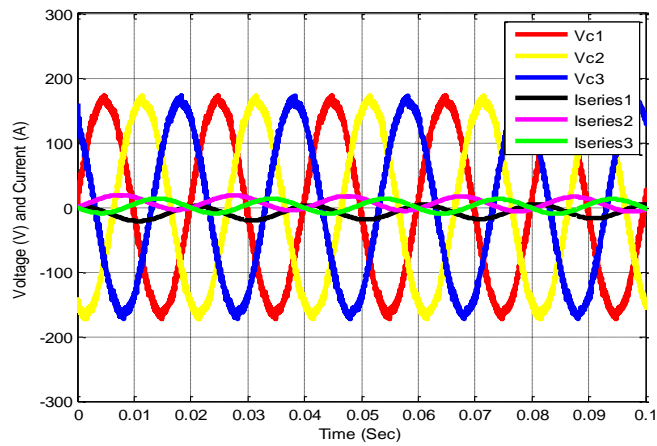


Figure-20. Plot of UPFC voltages and currents against time at the point of common coupling.
Source: Simulation result.

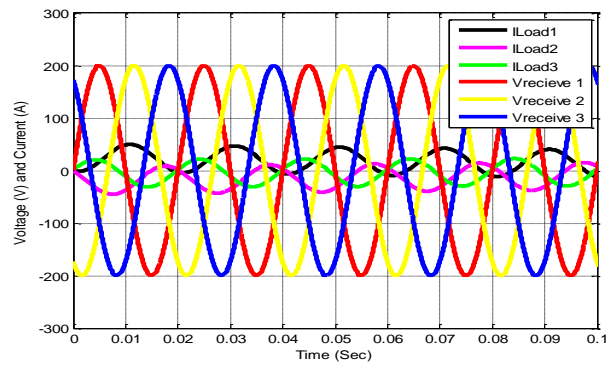


Figure-21. Plot of UPFC voltages and currents against time at the receiving end.
Source: Simulation result.

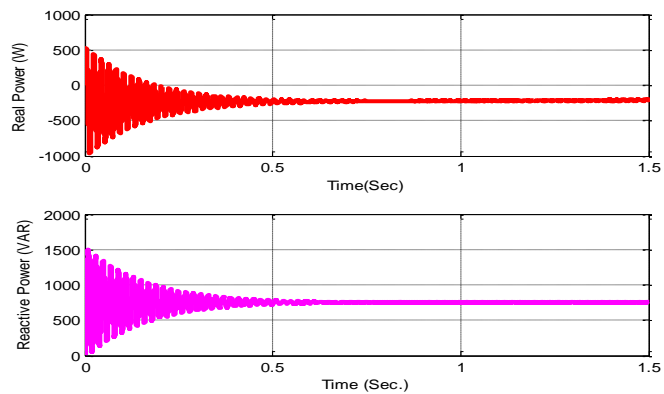


Figure-22. Plot of real and reactive power against time for the UPFC controller.
Source: Simulation result.

6. CONCLUSION

Three conventional FACTS-DEVICES have been modeled and simulated with respect to real and reactive power absorption and injection into the grid. The effects of a regulated thyristor angle on the thyristor conduction have been analyzed. The result analysis showed that thyristor controlled reactor absorbs more reactive power (0.875VAR) and injects more real power (2.575W) to the grid to compensates for the grid voltage drop through a

regulated firing angle of $0 \leq \alpha \leq \frac{\pi}{6}$. The static var compensator which has a superior characteristic over the

thyristor controlled reactor injects more reactive power of 28.75KVAR to the grid and absorbs a real power of 26.12KW. The unified power flow controller (UPFC) results indicates that lesser value of the real power (425W) is absorbed with a lesser value of a reactive power (675VAR) injected to the grid. This research paper has shown that a unified power flow controller is best applied for reduced load compensation.

Funding: This study received no specific financial support.

Competing Interests: The author declares that there are no conflicts of interests regarding the publication of this paper.

REFERENCES

- [1] C. O. Omeje, "Mathematical modeling and stability analysis of a hybrid five-level static VAR compensation for efficient power transmission," *International Journal of Engineering Trends and Technology*, vol. 63, pp. 17-27. Available at: <https://doi.org/10.14445/22315381/ijett-v63p204>.
- [2] C. Fuerte-Esquivel, E. Acha, and H. Ambriz-Perez, "A thyristor controlled series compensator model for the power flow solution of practical power networks," *IEEE Transactions on Power Systems*, vol. 15, pp. 58-64, 2000. Available at: <https://doi.org/10.1109/59.852101>.
- [3] N. G. Hingorani and L. Gyugyi, *Understanding FACTS concepts and technology of flexible AC transmission systems*. New York: Institute of Electrical and Electronic Engineers (IEEE) Publishers, 2000.
- [4] J. Arrillaga, B. C. Smith, N. R. Watson, and A. R. Wood, *Power System Harmonic Analysis*. Chichester: John Wiley and Sons, 1997.
- [5] J. Arrillaga and N. R. Watson, *Computer Modelling of Electrical Power System*, 2nd ed. Chichester: John Wiley and Sons, 2000.
- [6] O. Anaya-Lara and E. Acha, "Modeling and analysis of custom power systems by PSCAD/EMTDC," *IEEE Transactions on Power Delivery*, vol. 17, pp. 266-272, 2002.
- [7] L. K. Haw, M. S. Dahidah, and H. A. Almurib, "SHE-PWM cascaded multilevel inverter with adjustable DC voltage levels control for STATCOM applications," *IEEE Transactions on Power Electronics*, vol. 29, pp. 6433-6444, 2014. Available at: <https://doi.org/10.1109/tpel.2014.2306455>.
- [8] C. T. Lee, "Average power balancing control of a STATCOM based on the cascaded H-bridge converter with star configuration," *IEEE Transactions On Industrial Application*, vol. 50, pp. 3893-3901, 2014.
- [9] S. Du, J. Liu, J. Lin, and Y. He, "A novel DC voltage control method for STATCOM based on hybrid multilevel H-bridge converter," *IEEE Transactions on Power Electronics*, vol. 28, pp. 101-111, 2012. Available at: <https://doi.org/10.1109/tpel.2012.2195508>.
- [10] R. Xu, Y. Yu, R. Yang, G. Wang, D. Xu, B. Li, and S. Sui, "A novel control method for transformerless H-bridge cascaded STATCOM with star configuration," *IEEE Transactions on Power Electronics*, vol. 30, pp. 1189-1202, 2014. Available at: <https://doi.org/10.1109/tpel.2014.2320251>.
- [11] G. Farivar, B. Hredzak, and V. G. Agelidis, "Decoupled control system for cascaded H-bridge multilevel converter based STATCOM," *IEEE Transactions on Industrial Electronics*, vol. 63, pp. 322-331, 2015. Available at: <https://doi.org/10.1109/tie.2015.2472358>.

- [12] F. Shahnia, R. Rajakaruna, and A. Gosh, *Static compensators (STATCOMS) in power systems*. New York: Springer eBook, 2015.
- [13] G. Farivar, C. D. Townsend, B. Hredzak, J. Pou, and V. G. Agelidis, "Low-capacitance cascaded H-bridge multilevel StatCom," *IEEE Transactions on Power Electronics*, vol. 32, pp. 1744-1754, 2016. Available at: <https://doi.org/10.1109/tpel.2016.2557351>.
- [14] M. Saghaleini and H. Mirafrazi, "Reactive power control in three phase grid connected current source boost inverter," in *In Proceeding. IEEE Application on Power Electron Conference*, 2012, pp. 904-910.
- [15] Y. Liang and C. O. Nwakpa, "A new type of STATCOM based on cascading voltage source inverters with phase shifted unipolar SPWM," *IEEE Transactions Industrial Application*, vol. 32, pp. 1130-1138, 1996.
- [16] M. U. Agu, *Principles of power electronics circuits*, 1st ed. Enugu State Nigeria: University of Nigeria Press LTD, 2019.
- [17] V. Khadkikar, "Enhancing electric power quality using UPQC: A comprehensive overview," *IEEE Transactions on Power Electronics*, vol. 27, pp. 2284-2297, 2011. Available at: <https://doi.org/10.1109/tpel.2011.2172001>.
- [18] B. Han, B. Bae, H. Kim, and S. Bae, "Combined operation of unified power quality conditioner with distributed generation," *IEEE Trans. Power Electron*, vol. 13, pp. 315-322, 1998.
- [19] H. R. Mohammad, R. Y. Varjani, and H. Molchhari, "Multi-converter power quality conditioning system: MC-UPQC," *IEEE Transactions Power Delivery*, vol. 24, pp. 1679-1686, 2009.
- [20] V. Khadkikar and A. Chandra, "UPQC-S: A novel concept of simultaneous voltage sag/swell and load reactive power compensations utilizing series inverter of UPQC," *IEEE Transactions on Power Electronics*, vol. 26, pp. 2414-2425, 2011. Available at: <https://doi.org/10.1109/tpel.2011.2106222>.
- [21] A. M. Rauf, A. V. Sant, V. Khadkikar, and H. Zeineldin, "A novel ten-switch topology for unified power quality conditioner," *IEEE Transactions on Power Electronics*, vol. 31, pp. 6937-6946, 2015.
- [22] S. Yang, Y. Liu, X. Wang, D. Gunasekaran, U. Karki, and F. Z. Peng, "Modulation and control of transformerless UPFC," *IEEE Transactions on Power Electronics*, vol. 31, pp. 1050-1063, 2015. Available at: <https://doi.org/10.1109/tpel.2015.2416331>.
- [23] M. Basu, S. P. Das, and G. K. Dubey, "Comparative evaluation of two models of UPQC for suitable interface to enhance power quality," *Electric Power Systems Research*, vol. 77, pp. 821-830, 2007. Available at: <https://doi.org/10.1016/j.epsr.2006.07.008>.
- [24] V. Khadkikar and A. Chandra, "A novel structure of three phase four wire distribution system utilizing unified power quality conditioner (UPQC)," *IEEE Transactions Industrial Application*, vol. 45, pp. 1897-1902, 2009.

Views and opinions expressed in this article are the views and opinions of the author(s), Journal of Asian Scientific Research shall not be responsible or answerable for any loss, damage or liability etc. caused in relation to/arising out of the use of the content.